Modeling moisture distribution and binder migration in drying paper coatings

S. X. Pan, H. T. Davis, and L. E. Scriven

ABSTRACT: A consolidated paper coating is modeled as a three-dimensional network of 1000 pore bodies and interconnecting passages. The distributions of moisture and binder within a drying coating are examined using equations that describe the pore-level physics of meniscus-driven water flow, vapor diffusion, and binder transport and deposition. The model shows that pores do not dry exclusively from the surface into the coating unless the drying rate is extremely high. Rather, pore bodies usually empty in the order of their size and accessibility to the gas phase. The model includes two numbers that characterize binder transport in the coating: (a) a capillary number that describes the competition between capillary driving force of and viscous resistance to flow and (b) a Peclet number that describes the competition between convection toward and diffusion away from evaporating pores. The two numbers reflect effects of drying rate and binder diffusivity on binder migration.

KEYWORDS: Adhesive migration, bibliographies, coated papers, coatings, drying, equations, fluid flow, simulation.

The pattern of water movement, evaporation, and binder deposition in a drying paper coating is crucial to its pore structure *(1, 2)*, optical properties *(3)*, response to calendering *(4)*, and printing quality *(5)*. Laboratory measurements have shown that comparatively high drying rates promote migration of starch binder to the coating surface *(6)*. Latex binders have shown a similar trend *(7)*.

In an effort to improve coating qualities, researchers have attempted to correlate binder migration with the drying rate and its history. Despite the complexity of coating composition, pore structure, and coating–base-paper interaction, the mechanisms of drying and binder migration have been established *(8)*. Capillarity-driven liquid flow, binder diffusion, and convection determine how binder distributes. Nowicki *et al. (9)* used two-dimensional networks to simulate and analyze the pore-scale physics of a drying paper coating. Continuing in this line of investigation—with the aim of understanding liquid movement and binder migration in drying paper coatings—we developed a three-dimensional pore-scale network model to examine broader ranges of drying rate and binder diffusivity than occur in industrial practice.

Theory

Coating structure and network representation

Typical paper-coating formulas consist of pigment particles together with binders and additives in water. The volume fraction of particulate solids (including latex) typically exceeds 37%, and the mass fraction of total particulate and dissolved solids is over 60%.

Shortly after the layer of coating is deposited, drying begins. As water evaporates, the volume available for particle movement diminishes continuously until the coating consolidates. This is the point at which pigment particles make enough contacts with each other that they become fixed in their relative positions. The fluid-filled space among them is

Pan, researcher, Davis, professor, and Scriven, regent's professor, are active in the Coating Process Fundamentals Program, Center for Interfacial Engineering and Dept. of Chemical Engineering & Materials Science, University of Minnesota, 421 Washington Ave., SE, Minneapolis, MN 55455.

1. Network representation of a porous coating. **A**: magnification of a real coating; **B**: network representation of continuous pore space with average connectivity; **C**: converging–diverging doughnut-hole pore passage; **D**: connection of a cubic pore body with six neighboring pore passages.

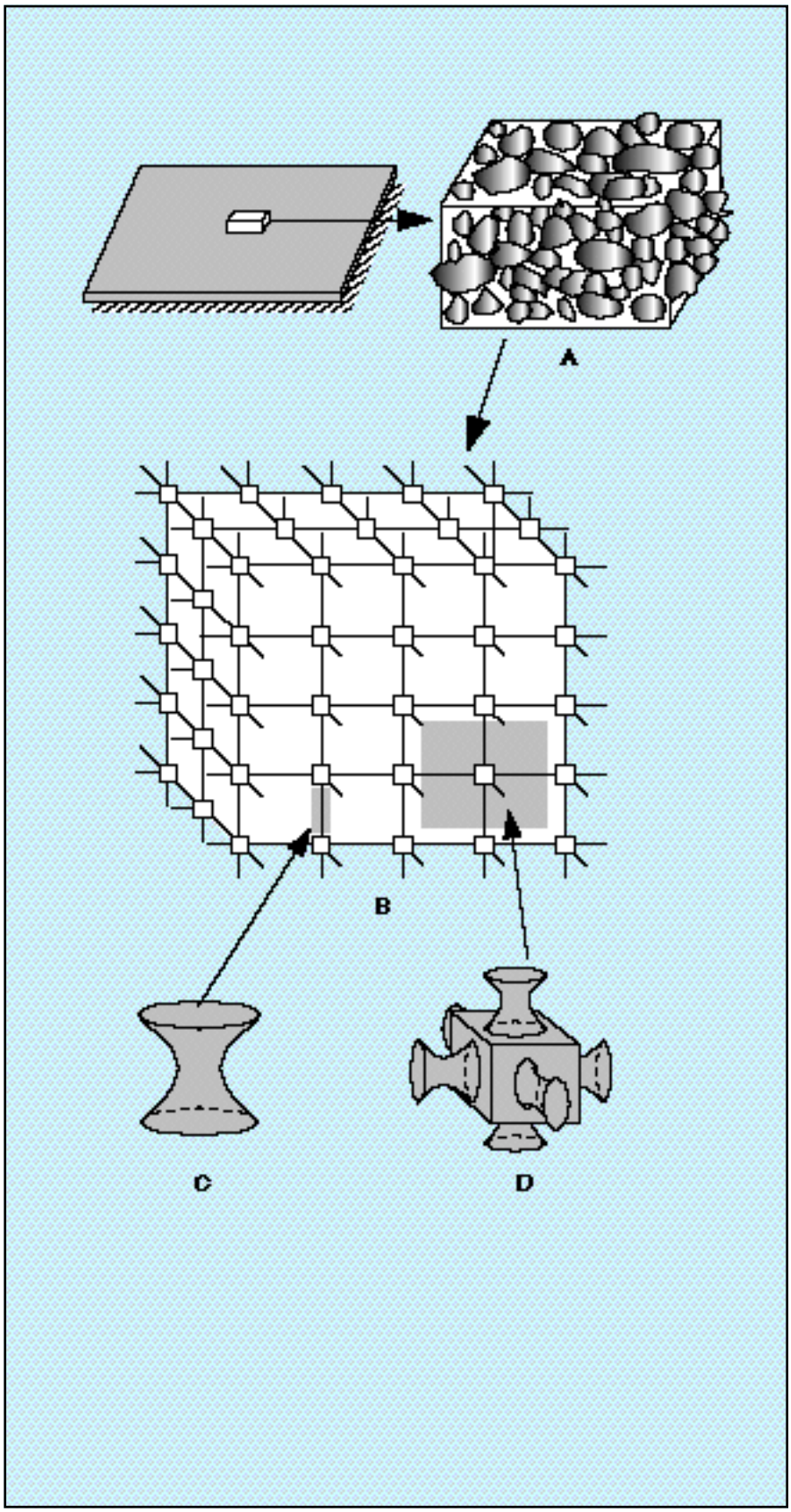

2. Capillary flow in a passage resulting from greater curvature of evaporating meniscus

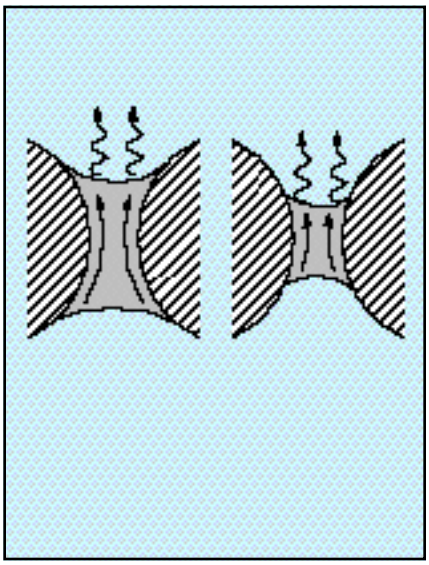

3. Rayleigh distribution of pore-throat radius

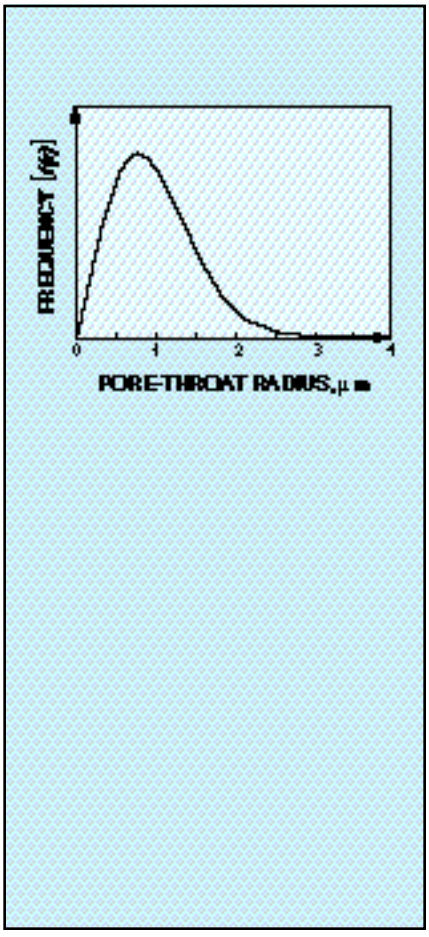

4. Capillary pressure profile across a meniscus moving from the top of the passage to the bottom as liquid recedes down the passage *(16)*

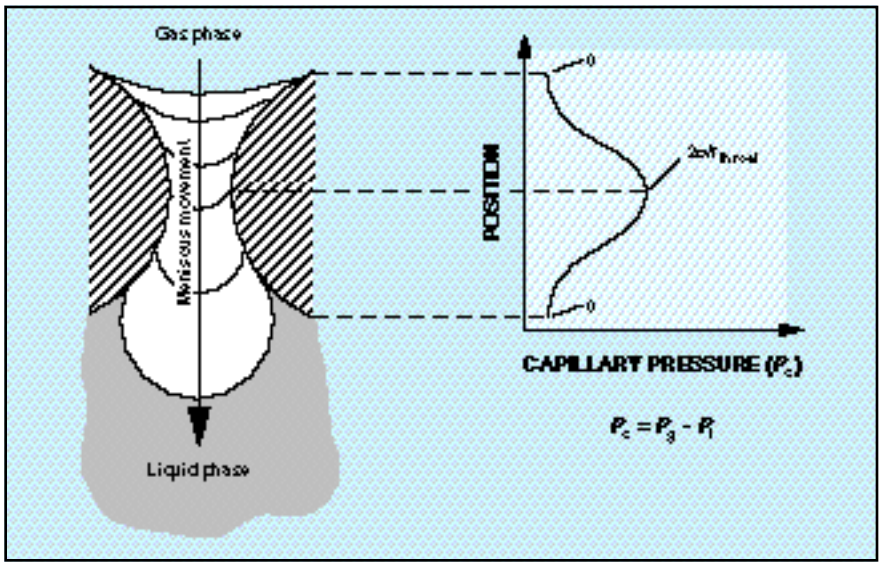

5. Illustration of drying mechanisms. **A**: Liquid flows › to the menisci, where liquid evaporates ∿➤. **B**: The fastest receding meniscus reaches a pore throat *. **C**: Haines jump causes liquid to flow away from the jumping meniscus, and the liquid cluster redistributes the liquid by adjusting its menisci. **D**: Drying continues and vapor diffuses away from evaporating menisci through old and new paths.

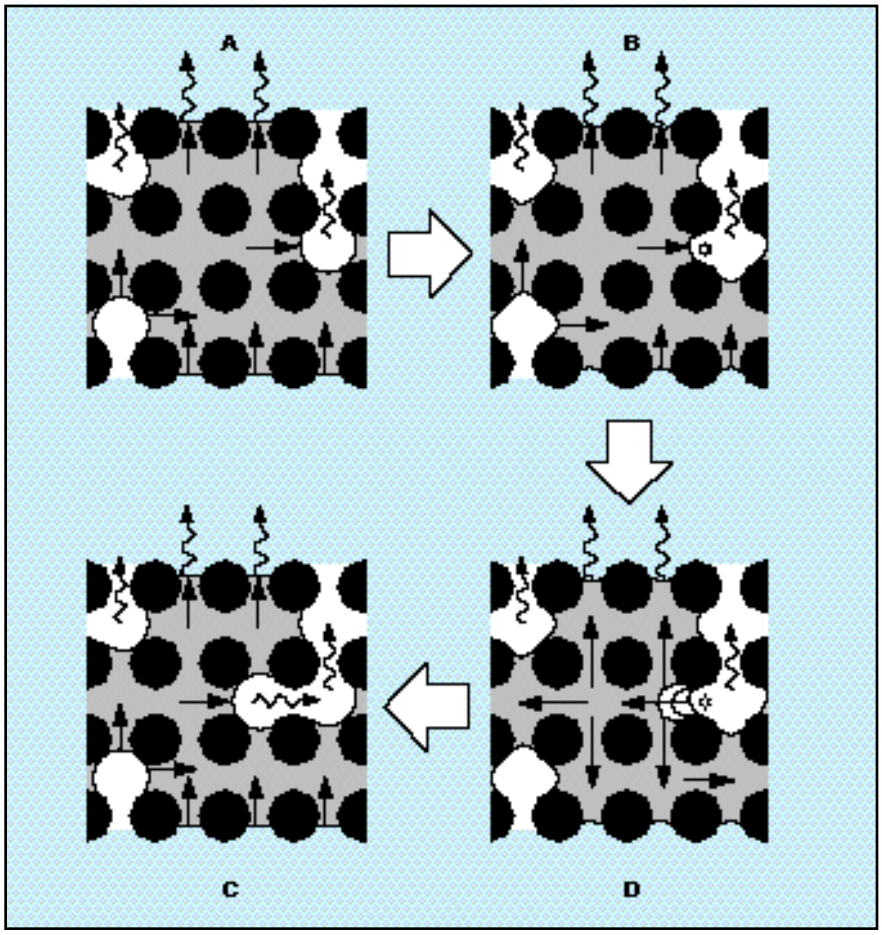

called pore space or void. Thus the coating microstructure can be viewed as a continuous solid matrix of connected pigment particles and an interpenetrating, continuous pore space between the particles.

The particle packing, and hence the pore structure, strongly depends on the shape, size distribution, and surface properties of particles as well as coating conditions and other components that may be present *(10)*. Hemstock and Bergmann *(11)* and Trader *(12)* have attempted without success to correlate coating porosity with clay size distribution. Climpson and Taylor *(13)* measured pore volume distribution with respect to pore size in paper coatings. Typically, the particle size is within the range 0.01–10 μm, and the void fraction rises as binder content falls in the range of 0.2 for board coatings to 0.5 for gravure printing. Pore sizes are usually on the order of the particles' sizes, i.e., they vary from submicrons to microns.

The pore space consists of constricted channels (pore passages) and enlarged junctions (pore bodies). Microscopy techniques have established that the connection of pores in a paper coating is highly irregular *(14)*. The coordination number, the number of ways out of a pore body, differs from one body to the next. Furthermore, depending on the particles surrounding it, a pore can vary greatly from the shape, size, and surface roughness of its neighbors. The pore walls can also be heterogeneous in composition, adsorptivity, and wettability. Despite the irregularity of the coating structure, advances in the science of porous media *(15)* have shown that fluid distribution, permeability, and other macroscopic properties of porous materials can be modeled satisfactorily with regular networks. The network's local properties are derived from the same distribution as the real pore space in the coating.

Our regular network representation is shown in **Fig. 1**. The solid

I. Parameters for normal drying conditions

	Definition	*Low*	*High*
Dimensional parameters			
W, kg/m^2·h	Initial drying rate	10^{1}	10^{2}
D_v, m^2/s	Diffusivity of vapor	10^{-5}	10^{-5}
D_b, m^2/s	Diffusivity of binder	10^{-15}	10^{-10}
μ, Pa·s	Liquid viscosity	10^{-3}	10^{-1}
σ, N/m	Surface tension of liquid	10^{-2}	10^{-1}
L, m	Coating thickness	10^{-5}	10^{-4}
r_2–r_1, m		10^{-9}	10^{-6}
Dimensionless parameters			
Bo	Bond number	10^{-6}	10^{-2}
Ca_{min}	Minimum capillary number	10^{-6}	10^{-2}
Ca_{max}	Maximum caplillary number	10^{-4}	10^{0}
Pe	Peclet number	10^{-1}	10^{6}
Sh	Sherwood number	10^{-2}	10^{0}

6. Illustration of binder-migration mechanisms. Because of the evaporation shown in Fig. 5A, binder in flowing liquid convects to the evaporating menisci →, where it is more concentrated (darker). Simultaneously, binder diffuses away from evaporating menisci against its concentration gradient ∿∿►.

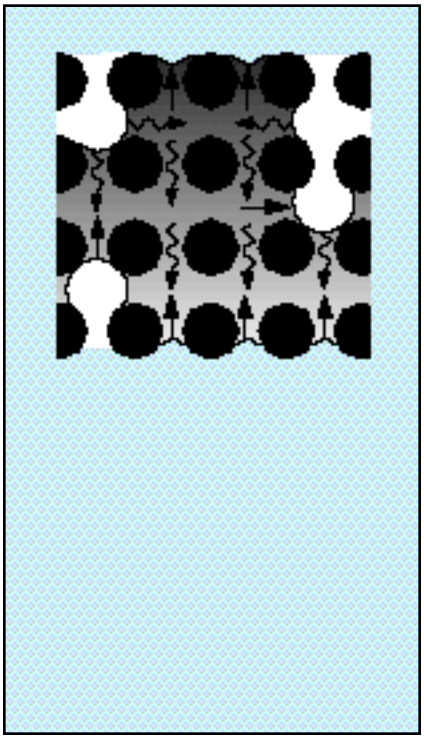

matrix and pore space are continuous and interpenetrating, as seen in Fig. 1B. The shape of the pore passage is chosen to account for the distribution and movement of menisci under the control of capillarity, to represent the resistance to liquid flow in the paper coating, and to allow efficient computation.

The bispherically curved (doughnut-like) shape in Fig. 1C is a simple representation of the converging–diverging character of pore passages *(16)*. **Figure 2** illustrates the capillary action of menisci within a passage. Because local flow resistance varies inversely as the fourth power of pore radius, the narrow pore throat dominates the resistance to liquid flow. The pore spaces empty by Haines jumps—where the emptying occurs at a bound—so they have a much less important role in resisting liquid flow. It is convenient to model the bodies as cubes onto which the pore passages are fused, as seen in Fig. 1D. The models of pore passages and pore bodies could be modified to account for special pore structures. We chose the coordination number of the three-dimensional network to be six, as if the particle packaging were simple cubic. However, the coordination number can be adjusted to any average value exhibited by a particular paper coating by randomly removing or adding bonds between neighboring pore bodies.

Once the network representation is set up, it has to be decorated with sizes and with physical and chemical properties. The radii of the pore throats were drawn from statistical distributions illustrative of those in paper coatings. The side lengths of each pore-body cube were chosen to be the largest pore diameter of the pore passages terminating in the pore body. Pore-passage length and pore-body volume then were calculated. If statistical distributions of each of these parameters are available, they should be used to decorate the network.

The pore-throat radii in the network are from a Rayleigh distribution truncated at 0.3 μm and 1.3 μm, with a mean radius of 0.8 μm. The Rayleigh distribution is illustrated in **Fig. 3**. The network of 10 x 10 x 10 pore bodies corresponds to about 60 μm x 60 μm x 60 μm. By using so-called periodic boundary conditions on each pair of opposed lateral faces of this small sample, we multiplied it into a much larger sample. We took the solid matrix to be rigid, nonswellable, and inert. These restrictions could be relaxed, in particular to account for changes in coating structure during drying and for pigment interaction with solvents, binders, and additives.

7. Drying-rate curves (dimensionless drying rate is in units of the initial drying rate)

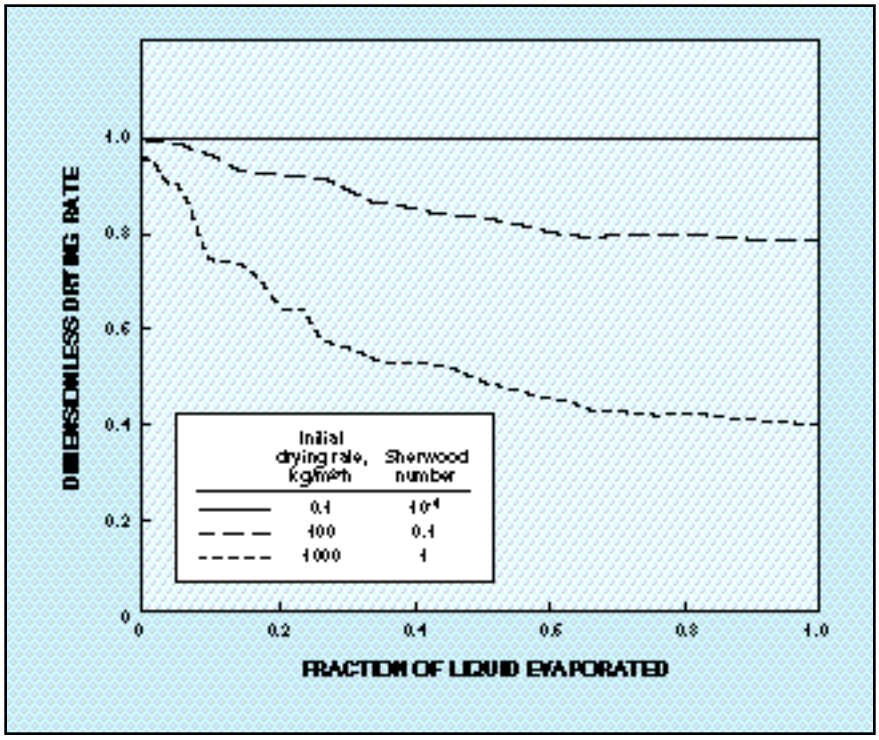

Drying of a paper coating

Mechanisms. Drying of porous media has been studied intensively, mainly in soil science, forest products, chemical engineering, and food science. A drying process can be phenomenologically divided into three periods *(17)*:

1. Constant-drying-rate period, during which the rate of evaporation is nearly independent of the moisture content
2. First falling-rate period, during which the rate of drying is often close to a linear function of the moisture content
3. Second falling-rate period, during which the rate of drying is distinctly not linear in moisture content.

However, observed drying-rate curves strongly depend on the type of material and drying conditions *(18)*.

Great efforts have been made to develop drying theories that account for the observed phenomena. The limitations of moisture-diffusion theory have been recognized since 1934, when Sherwood pointed out that capillarity is important in drying clays *(19)*. Capillary theory developed in soil science and hydrology was brought to the attention of chemical engineers in 1937 by Ceaglske and Hougen *(20)*. In 1966, Luikov developed a theory for mass and heat transfer in capillary–porous bodies based on irreversible thermodynamics *(21)*. However, these theories embody moisture-content-dependent transport parameters that are difficult to measure, much less to predict, especially for a thin layer of paper coating. Moreover, these theories do not distinguish locally between vapor and liquid water, and thus do not consider transport through menisci within the pore space.

Volume-averaging theory recognizes pore space and starts with fundamental fluid-transport equations of confined, continuous phases *(22)*. However, the averaging process loses pore-space topology and geometry, and with them the connectivity and flow of liquid. A paper coating is so thin in one direction as to defy assigning it the representative elementary volume and the representative elementary area (associated with menisci) called for by the theory, because these should be much larger than the pore size yet much smaller than the overall size of the porous material.

The mechanisms of fluid transport within a drying porous medium have been established *(18)*. In the constant-rate period, liquid flows to the surface of the porous medium, where it evaporates, or else the external resistance of the flowing gas to mass transfer is controlling whatever is happening within the pore space. In the falling-rate periods, liquid evaporates within the material and vapor diffuses out through gas-filled pore space. As a meniscus of wetting liquid descends into a converging–diverging passage (pore throat), the situation is stable as long as the meniscus resides in the converging section. This is so because the liquid pressure behind the meniscus falls as it advances and becomes more sharply curved, as illustrated in **Fig. 4**.

At this stage, liquid flows from nonevaporating or slower evaporating menisci to faster evaporating ones, as seen in **Fig. 5**. The menisci in all pore passages steadily recede from pore bodies toward pore throats. When a meniscus reaches a pore throat (asterisk in Fig. 5B), the situation there becomes unstable. At this point, capillary action propels the meniscus through the diverging section and liquid-occupied pore bodies until it lands at a new stable posi-

II. Equations of network model during continuous movement of menisci

Equation	*Eq. no.*	*Comments*
Stokes flow from pore body i to adjacent pore body or meniscus j		
$q_{ij} = (g_{ij}/\mu)/(P_i - P_j)$	(1)	Liquid volumetric flow rate
$g_{ij} = \pi r_{ij}^4/8l_{ij}$	(2)	Liquid flow conductance
$P_j = P_a - (2\sigma/R_j)$	(3)	Young–Laplace equation of liquid pressure beneath the meniscus
Vapor diffusion and convection		
$dm_{ij}/dt = \pi r_{ij}^2(P_a M_v D_v/RTl_{ij})\{\ln[(P_a - p_j)/(P_a - p_i)]\}$	(4)	Vapor mass rate of diffusion and convection induced by diffusion, from pore body i to adjacent pore body or meniscus j
$dm_{ia}/dt = \pi r_{ia}^2 k_{m,i}(p_i - p_a)$	(5)	Vapor mass-transfer rate at coating surface from pore body or meniscus i to air a
$m_i = M_v RT/p_i V_i$	(6)	Perfect gas law relation between mass and partial pressure of vapor in pore body i
Binder diffusion and convection from a pore body j to adjacent pore body or meniscus i		
$dm_{d,ij}/dt = \pi r_{ij}^2[(M_b D_b)/l_{ij}]\,(c_j - c_i)$	(7)	Binder mass diffusion rate
$dm_{c,ij} = M_b c_i q_{ij}$ (for $q_{ij} > 0$)	(8a)	Binder convection rate with
$dm_{c,ij} = M_b c_j q_{ij}$ (for $q_{ij} < 0$)	(8b)	flowing liquid
$c_i = m_i/V_{i,l}$	(9)	Relation between binder mass, liquid volume, and concentration in pore body or meniscus-laden pore passage i
if $c_i \geq c_{sat}$, then $c_i = c_{sat}$ and binder deposits		Binder deposition condition
Mass balance equations		
$-\sum_{j=1}^{n} q_{ij} = 0$	(10)	No liquid accumulation in liquid-filled pore body i
$dm_i/dt = -\sum_{j=1}^{n} (dm_{ij}/dt)$	(11a)	Vapor accumulation in gas-filled pore body i in the
$dm_i/dt = [(dm_{ij}/dt) - (dm_{ia}/dt)]$	(11b)	coating (11a) or on the surface (11b)
$dm_j/dt = -\sum_{j=1}^{n-1} \rho_l q_{ij} + (dm_{kj}/dt)$ (for $i \neq k$)	(12a)	Liquid and vapor accumulation in meniscus-laden
$dm_j/dt = \rho_l q_{ij} - (dm_{ja}/dt)$	(12b)	passage j in the coating (12a) or on the surface (12b)
$dm_j/dt = \sum_{i=1}^{n} (dm_{d,ij}/dt) + (dm_{c,ij}/dt)]$	(13)	Binder accumulation in liquid-filled pore body j
$dm_j/dt = [(dm_{d,ij}/dt) + (dm_{c,ij}/dt)]$	(14)	Binder accumulation in meniscus-laden pore passage j

tion (Fig. 5C). This event is called a Haines jump, named for the scientist who observed "unstable stages at which filling or emptying is completed at a bound" with a light microscope in 1930 *(23)*. After a Haines jump, the liquid cluster or clusters involved adjust their menisci to accommodate the liquid from the evacuated pores, as illustrated in Fig. 5D.

No previous macroscopic drying theory has taken Haines jumps into account. Following the initiation of this theory *(9)*, we have installed the pore-level physics of meniscus action, water flow, and vapor diffusion in a three-dimensional network model of paper coating, as detailed in the preceding section. This model was validated by comparing its predictions for two-dimensional samples with those of our earlier two-dimensional network model, which used biconical pores rather than doughnut-hole pores *(9)*. The two sets of predictions agreed with each other. Using doughnut-hole passages eliminates intervals in which a meniscus remains pinned to the sharp-edged end and throat, thereby making computation more efficient.

Liquid flow in a paper coating. The liquid flow is driven by pressure

III. Equations of network model during Haines jump

Equation	Eq. No.	Comments
Haines jump condition for meniscus i in its passage		
$R_i \le r_i$	(15)	Lower limit for meniscus radius R_i at a pore-throat of radius r_i
Controlling equation during Haines jump (for each liquid cluster sum over all menisci)		
$\sum_{menisci}(\Delta V) - \Delta V_{dist.} = 0$	(16)	Constant liquid volume in each liquid cluster during jump
Radius of meniscus at the end of Haines jump (for each liquid cluster)		
$R_{i1} = R_{i2} = \ldots = R_{ci}$	(17)	All menisci in a liquid cluster have the same curvature
Relation of liquid volume V_i and radius of spherical meniscus i in a "doughnut-hole" pore passage		
$V_i = V_{bi} - V_{si} - V_{ei} + V_{pi}$	(18)	
$V_{bi} = \pi l_i^2\{\pi r_i + l_i[(\pi - 4/3)]$		
$V_{si} = \pi A_i^2(3R_i - A_i)$		
$V_{ei} = \pi\,(l_i + r_i)^2 l_i[(R_i - r_i)/(R_i + l_i)]$		
$V_{pi} = 2\pi\{[(r_i + R_i)\sin^{-1}(B_i/R_i)] + [(R_i^2 - B_i^2)^{3/2}/3] + U_i\}$		
$U_i = (r_i + R_i)B_i\{[(R_i^2 - B_i^2)^{1/2}/2] - C_i\} + B_iC_i - (R_i^3/3)$		
$A_i = R_i(1 - \{1 - [(l_i + r_i)/(l_i + R_i)]^2\}^{1/2})$		
$B_i = l_i[(R_i - r_i)/(R_i + l_i)]$		
$C_i = l_i\{1 - [(l_i + r_i)/(l_i + R_i)]^2\}^{1/2}$		

IV. Summary of cases

	Case 1 [a]	Case 2 [b]	Case 3 [c]	Case 4 [d]	Case 5 [e]
Dimensional parameters					
W, kg/m²·h	10^{-1}	10^{3}	10^{-1}	10^{3}	10^{2}
D_v, m²/s	10^{-5}	10^{-5}	10^{-5}	10^{-5}	10^{-5}
D_b, m²/s	10^{-16}	10^{-12}	10^{-10}	10^{-6}	10^{-7}
μ, Pa·s	10^{-3}	10^{-3}	10^{-3}	10^{-3}	10^{-3}
σ, N/m	10^{-1}	10^{-1}	10^{-1}	10^{-1}	10^{-1}
Dimensionless parameters					
Ca_{min}	10^{-5}	10^{-1}	10^{-5}	10^{-1}	10^{-2}
Ca_{max}	10^{-2}	10^{2}	10^{-2}	10^{2}	10^{1}
Pe	10^{3}	10^{3}	10^{-3}	10^{-3}	10^{-3}
Sh	10^{-4}	10^{0}	10^{-4}	10^{0}	10^{-1}

[a] Case 1: slow initial drying, low binder diffusivity
[b] Case 2: fast initial drying, low binder diffusivity
[c] Case 3: slow initial drying, high binder diffusivity
[d] Case 4: fast initial drying, high binder diffusivity
[e] Case 5: fast initial drying, high binder diffusivity

gradient and, to a negligible extent, by gravity. Flow is resisted by viscosity. During drying, the pressure gradient is produced by capillarity, the action of surface tension in curved menisci. Liquid flows from less curved toward more curved menisci. Thus the volumetric flow rate between two pore bodies, q_{ij}, can be defined as follows:

$$q_{ij} \propto (2\sigma_j/R_j) - (2\sigma_i/R_i)$$

where

σ = surface tension of the liquid (here, $\sigma_j = \sigma_i = \sigma$ for the sake of simplicity)

R = mean radius of curvature of each meniscus ($R_i > R_j$).

The maximum liquid pressure difference, $P_i - P_j$, can be estimated by using minimum and maximum throat radii in place of R_i and R_j. Likewise, the minimum capillary pressure difference can be estimated from the two closest radii.

The ratio of gravitational to surface tension or capillary forces is called the Bond number, Bo.

$$\mathrm{Bo} \equiv [g_L(\rho_l - \rho_g)L\, r_1\, r_2]/\,[2\sigma(r_2 - r_1)]$$

where

g_L = local acceleration of gravity

8. Liquid distribution at 50% saturation during slow drying (initial rate of 0.1 kg/m^2·h). Vapor is swept away by flowing air on the top. The coating rests on a porous substrate, the effect of which is neglected.

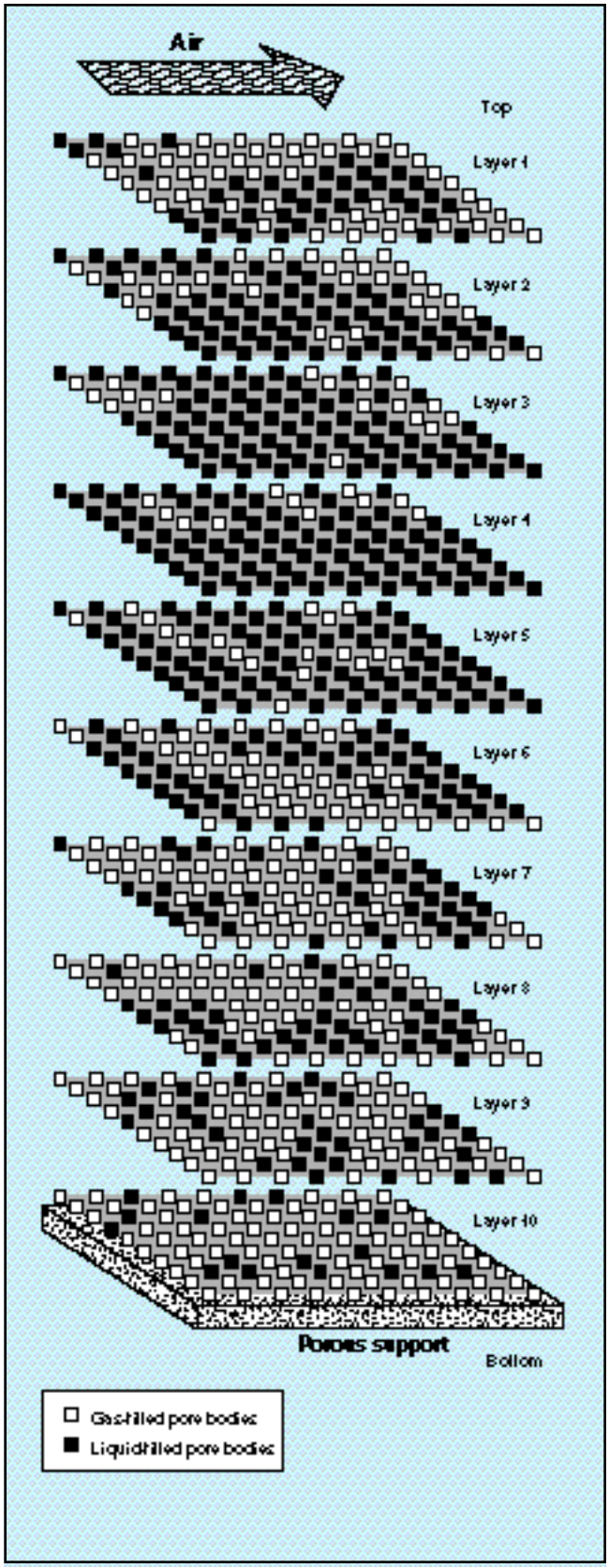

9. Liquid distribution at 50% saturation during fast drying (initial rate of 1000 kg/m^2·h) in the same coating as Fig. 8

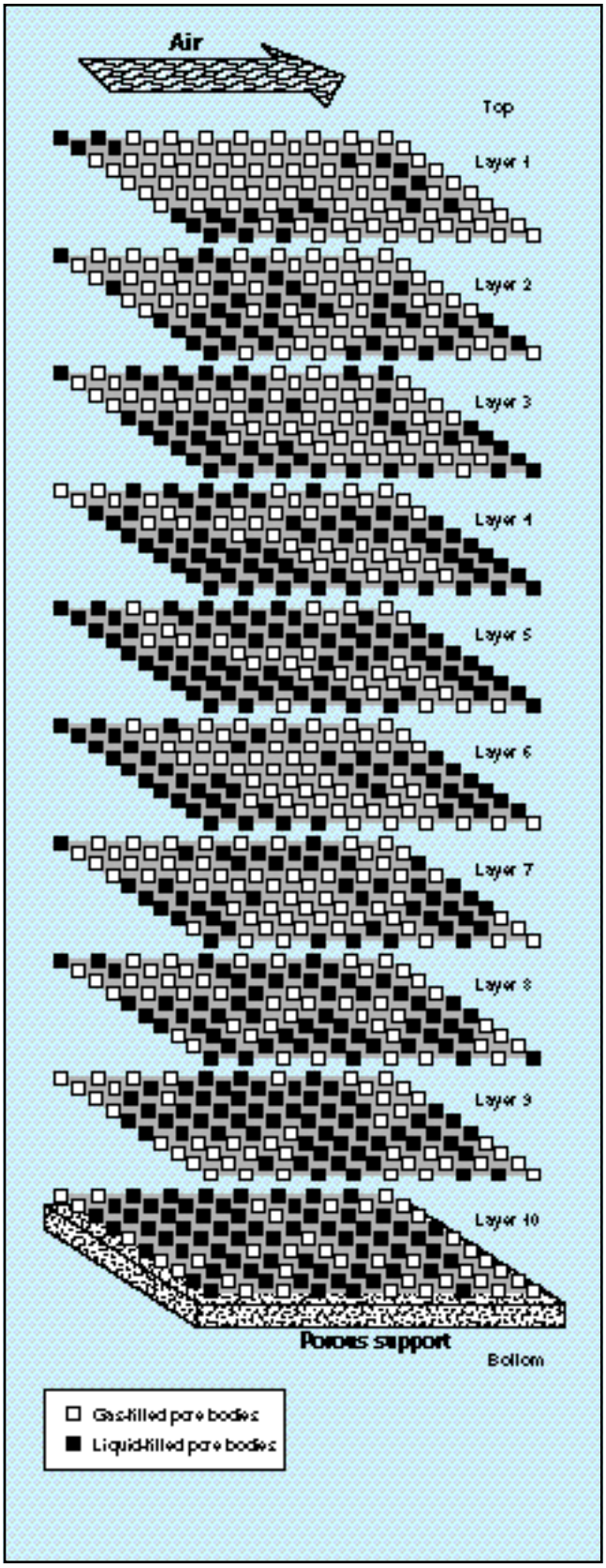

ρ_l = density of liquid

ρ_g = density of gas

L = coating thickness

r = pore-throat radius

In a coating with pore sizes ranging from 0.1 μm to 10 μm, with an average of 1 μm, the Bond number varies from 10^{-6} to 10^{-2}. (Other parameters for normal drying conditions are given in **Table I**.) Thus in thin coatings, the effect of gravity is quite insignificant. It follows that at mechanical equilibrium, menisci in a liquid cluster surrounded by atmospheric gas all have the same curvature. After a Haines jump, the nearby menisci tend to be close to mechanical equilibrium. As a reasonable approximation, they can all be taken to be at mechanical equilibrium.

The evaporation of liquid in a meniscus-laden passage causes the meniscus to migrate toward the pore throat. As it does so, its curvature rises and the resultant lowered pressure draws liquid from the less-curved menisci within the same liquid cluster (connected liquid). Menisci in smaller passages can stand up to lowered pressure, so Haines jumps tend to take place in the larger passages occupied by menisci.

The capillary-pressure-difference-driven flow is resisted by viscosity. If the viscous resistance is large enough, liquid can flow very slowly, and it can take a long time to reach mechanical equilibrium. This competition can be described by a capillary number, Ca, the ratio of viscous resistance to capillary driving force.

$$Ca \equiv (\mu WL)/[\sigma \rho_l r_2 (1 - ß)]$$

where

μ = liquid viscosity

W = initial drying rate or mass-transfer coefficient on the coating surface

ß = pore size ratio, r_1/r_2.

The effect of the capillary number on the liquid distribution is examined later in this report.

The inertia of the flow is far less than the net viscous force, i.e., the Reynolds number, Re,

$$Re \equiv 2Wr_{ij}/\mu$$

is much less than unity. In a drying paper coating, Reynolds number is less than 10^{-3}, even at a drying rate, W, of 1000 kg/m²·h and liquid viscosity, μ, of 10^{-3} Pa·s. Consequently, the volumetric flow rate, q_{ij}, between two adjacent liquid-filled pore bodies is proportional to the pressure difference, $P_i - P_j$, and inversely proportional to the liquid viscosity *(24)*. The proportionality factor is the flow conductance, g_{ij}, which depends on the shape and size of the pore section. The conductance is known for some model pore sections. For a cylindrical tube of length l and radius r:

$$g = \pi r^4/8l$$

For an orifice:

$$g = r^3/3$$

For a hyperboloid:

$$g = \pi r^3/3f(l/r)$$

where $f(l/r)$ is a function of the aspect ratio l/r. For a doughnut-hole passage, we chose to use

$$g_{ij} = \pi r_{ij}^4/8l_{ij}$$

in lieu of an accurate evaluation of $f(l/r)$. Here r_{ij} is the radii of pore throat between pore bodies i and j, and l_{ij} is the passage length between the pore bodies. The flow rate between a meniscus in a passage and a nearby liquid-filled pore body can be similarly derived.

Vapor transfer. At an evaporating meniscus or gas-filled pore body near the top of the coating, the mass-transfer rate is proportional to the partial-pressure difference between the pore and the ambient gas phase far from the coating surface. The proportionality constant is the mass-transfer coefficient at the coating surface (Eq. 5 in **Table II**), which depends on the nature of gas flow, gas flow rate and direction, heating method, and other dryer conditions. The initial drying rate is the sum of the mass-transfer rates from the menisci on the top at the beginning of drying of liquid-saturated coating.

Transport in the gas phase is by vapor diffusion, convection induced by evaporation, and convection induced by diffusion. The evaporative convection inside a paper coating is negligible because the vapor Peclet number, Pe_v, is small, even at high drying rates.

$$Pe_v \equiv WL/\rho_l D_v$$

where

D_v = diffusivity of vapor.

Convection induced by diffusion is important only in a pore space near evaporating menisci where liquid temperature is close to the boiling point. Consequently, we considered diffusion and convection induced by diffusion as vapor transfer through a stagnant gas phase *(25)*. For the sake of simplicity, we use the term diffusion to describe both diffusion and convection induced by diffusion.

The mass diffusion rate between adjacent gas-filled pore bodies or between an evaporating meniscus and a gas-filled pore body is proportional to the diffusivity of vapor, the partial-pressure difference of vapor in the gas, and the cross-section area (Eq. 4 in Table II). The Kelvin effect, which relates the equilibrium vapor pressure above a meniscus and the meniscus curvature, is negligible in pores of relevant size and therefore has been ignored, although it could readily be included. The effect here on the liquid distribution would be very small unless the coating were drying under near-equilibrium conditions, where capillary condensation would be significant.

The equations of liquid flow and vapor transfer are mass balances at pore passages and pore bodies. Because there is no net change of liquid content in each liquid-filled pore body,

10. Deposition of binder (diffusivity = 10^{-6} m^2/s) at drying rate 1000 $kg/m^2 \cdot h$ (Case 4 in Table IV). **A:** top two layers at 48% liquid saturation; **B:** top two layers at zero liquid saturation (dried coating); **C:** bottom two layers at zero liquid saturation.

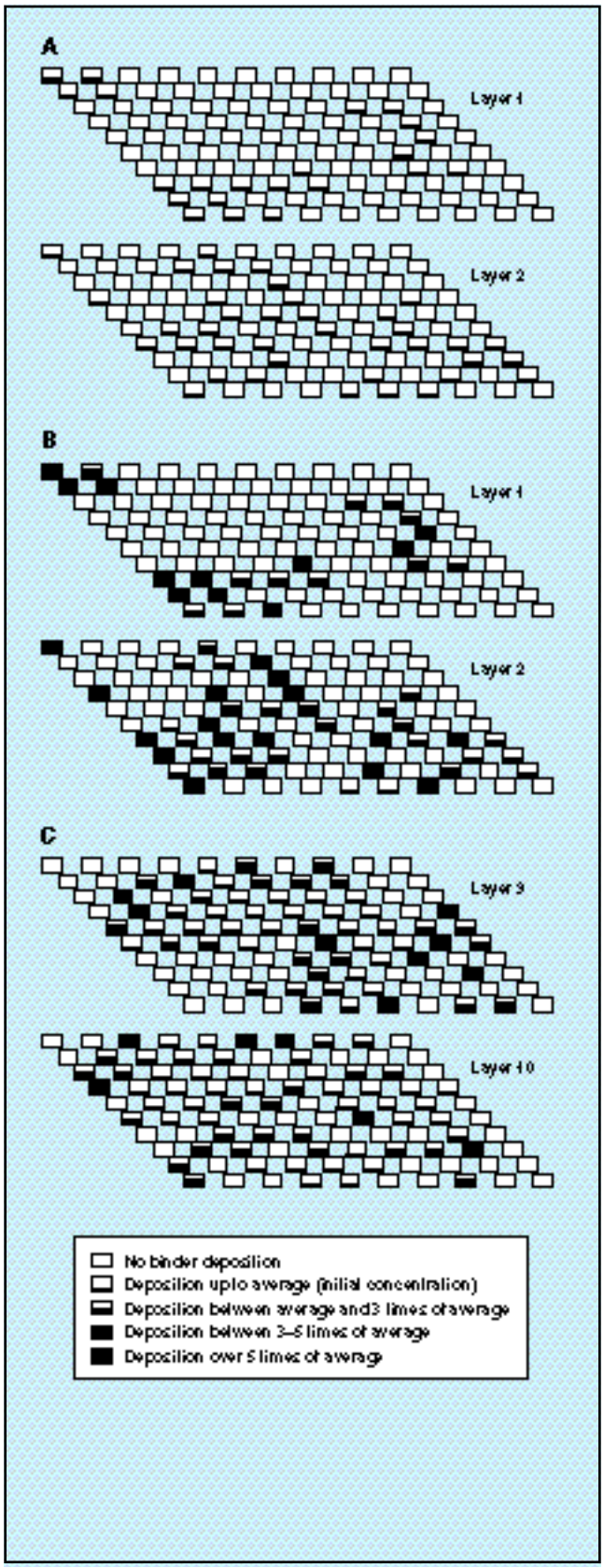

11. Deposition of binder (diffusivity = 10^{-10} m^2/s) at drying rate 0.1 $kg/m^2 \cdot h$ (Case 3 in Table IV). **A:** top two layers at 48% liquid saturation; **B:** top two layers at zero liquid saturation (dried coating); **C:** bottom two layers at zero liquid saturation.

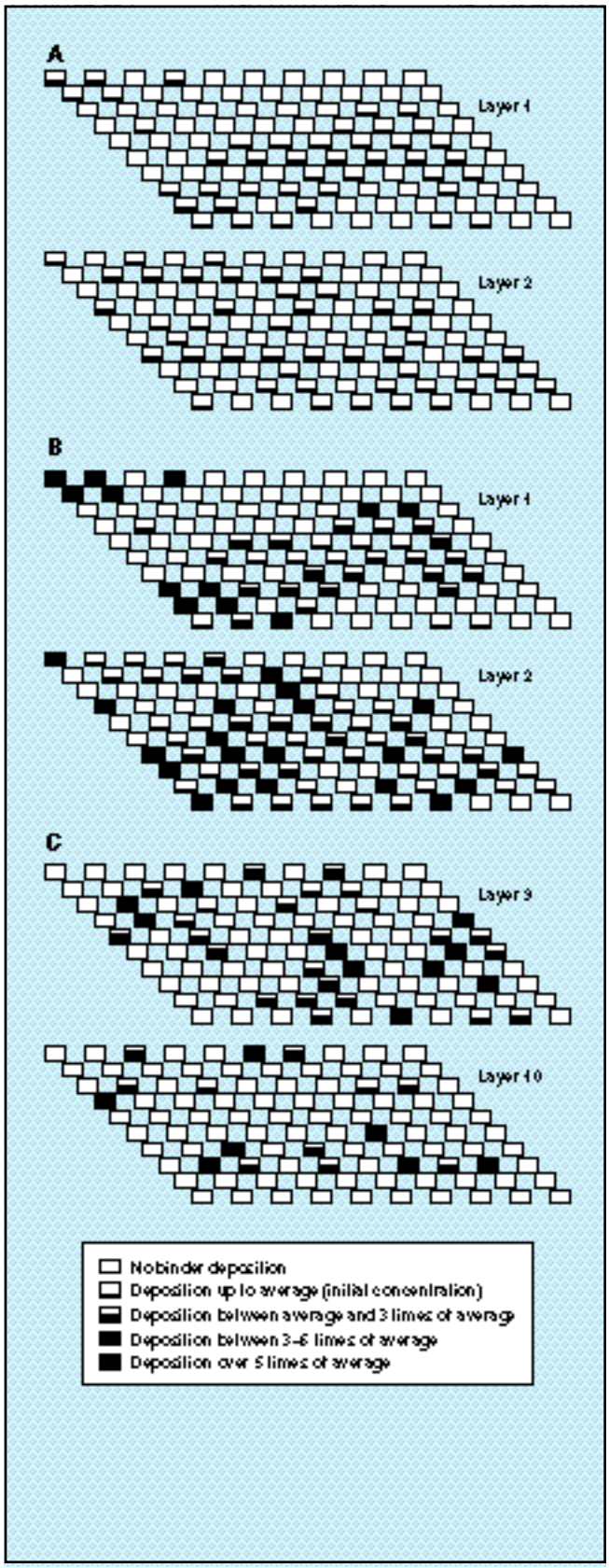

$$\sum_{j=1}^{n} q_{ij} = 0$$

This equation is essentially Kirchhoff's current law and is a special form of the general conservation of volume of incompressible fluid. The rate of change of liquid content in a meniscus-laden passage j (Eq. 12 in Table II) must equal the sum of the liquid inflow rate, ρq_{ij}, and the liquid evaporation rate, dm_{kj}/dt. The rate of change of vapor mass in a gas-filled pore body must equal the sum of vapor influx from neighboring pore space.

Binder migration in a drying paper coating

In pigmented coatings, the drying conditions can strongly affect how dissolved or suspended binder moves and distributes *(26, 27)*. It appears that print mottle in coated papers is likely a consequence of nonuniform deposition of binder on and near the coating surface *(28)*. It has been observed, for example, that using infrared radiation as well as air convection to achieve high drying rates promotes migration and consequent maldistribution of starch and latex binders *(6, 7, 27)*.

Hagen *(26)* identified two competing transport mechanisms of soluble binder. The competing mechanisms are illustrated in **Fig. 6**. Binder is convected with the water toward evaporating menisci, where it is left behind because it is not volatile. Simultaneously, binder diffuses back down the concentration gradient it has created, i.e., it diffuses against the flow. Once the concentration of binder behind the evaporating meniscus reaches the saturation value, the binder precipitates in the pore space. The competition between convection and diffusion is characterized by a Peclet number for binder.

$$\mathrm{Pe}_b \equiv WL/\rho_l D_b$$

where

D_b = diffusivity of binder.

Thus the lower the drying rate, or the higher the binder diffusivity, the more it tends to concentrate throughout each connected cluster of liquid-filled pores before it deposits.

These two competing mechanisms of binder migration are not the entire story. If the binder is particulate latex, frictional drag against pore walls may retard the convection. To a first approximation, however, the colloidal latex is much smaller than pore size, and friction can be ignored. Rather than depositing on surfaces, latex could flocculate within the pore space. By depositing at the meniscus, latex particles may cause much more sharply curved, smaller menisci to form in their interstices before they coalesce, so that the capillarity force is enhanced there. Whereas latex particles may flocculate and coalesce, soluble binder may gel or skin before it deposits. Either way, the passages may be occluded so that drying is greatly slowed. Other components in a coating blend can affect binder diffusion *(25)*. Lacking information about this from the literature, we adopt the binary diffusion approach, i.e., all cross diffusivities of a multicomponent system are set to zero. Moreover, the effects of any other additives on the drying process and binder migration are neglected. That is, we consider only a binary system of binder and water in the coating pore space and only the processes of binder convection and diffusion.

Soluble binders like starch are more mobile than colloidal particulate binders like polymer latex. The effect of mobility is reflected in its diffusivity, i.e., the less-mobile latex has smaller diffusivity. Binder diffusion coefficients vary with local concentration and temperature, which generally are changing during drying. Data on the ways they change are still scarce. Although theories of diffusion in polymer solutions are available, notably the free-volume theory of concentration-dependent diffusion coefficients, the material parameters called for by these theories are rarely available. Consequently, we have taken the diffusion coefficients to be constant during drying, although they certainly depend on the polymer concentration. Earlier results of two-dimensional modeling *(29)* showed that temperature ordinarily changes no more than a few degrees during the drying of unbound water from a thin coating. Therefore, it is reasonable to assume that the temperature of a coating remains constant as it dries out. This simplification can be removed. So can the neglect of viscosity change and surface-tension variation, though these may actually change a few orders of magnitudes during drying.

The equations of binder migration during drying represent that when liquid flows in pore space from i to j, the binder convection rate (Eq. 8a in Table II) is

$$dm_{c,ij}/dt = q_{ij} c_i M_b$$

where

c = concentration of binder

M_b = molecular weight of binder.

The binder diffusion rate (Eq. 7 in Table II) between these two places (i to j) is proportional to its concentration difference. The net mass rate of change of binder in a liquid-filled pore passage or pore body is the sum of the net fluxes by convection and by diffusion.

Equation system

The complete set of equations is summarized in **Tables II and III**. The backbone of the set consists of mass-balance equations for the liquid, the vapor, and the binder. The unknowns are meniscus curvature in meniscus-laden passages, liquid pressure in liquid-filled pore bodies, vapor partial pressure in gas-filled pore bodies, and binder concentration in meniscus-laden pore passages as well as liquid-filled pore bodies.

The network is initially filled with

12. Deposition of binder (diffusivity = 10^{-16} m^2/s) at drying rate 0.1 $kg/m^2 \cdot h$ (Case 1 in Table IV). **A:** top two layers at 48% liquid saturation; **B:** top two layers at zero liquid saturation (dried coating); **C:** bottom two layers at zero liquid saturation.

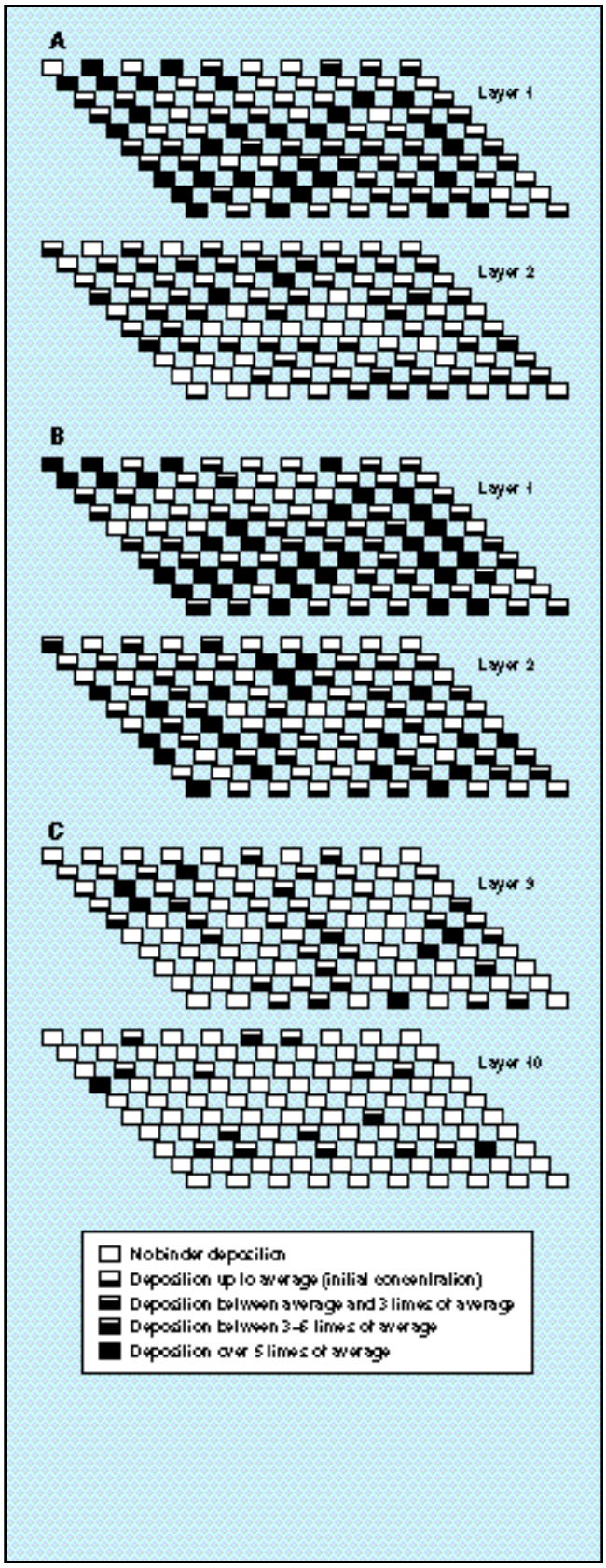

13. Deposition of binder (diffusivity = 10^{-12} m^2/s) at drying rate 1000 $kg/m^2 \cdot h$ (Case 2 in Table IV). **A:** top two layers at 48% liquid saturation; **B:** top two layers at zero liquid saturation (dried coating); **C:** bottom two layers at zero liquid saturation.

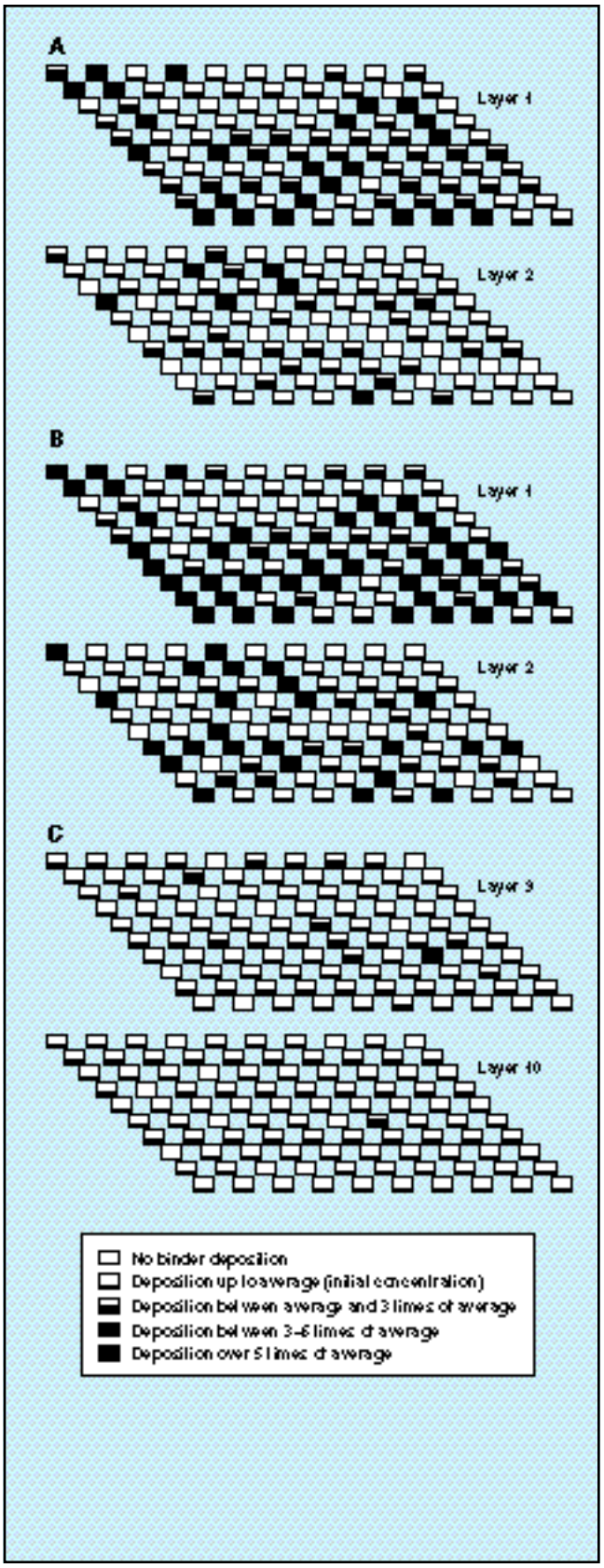

liquid in all pore bodies and pore passages. Dewatering of the coating by base paper is ignored—the network model is applied to consolidated coating initially full of water. The rate of drying from the bottom of the coating through the substrate is taken to be negligible compared with the rate from the top. Periodic boundary conditions are applied to the other two pairs of opposite boundaries, as previously noted in the discussion of "network representation."

Initially, all the menisci at top and bottom are flat and so have the same curvature. The initial binder concentration is 50% of its saturation value throughout the pore space. After each jump, liquid from the evacuated pore is immediately redistributed in the liquid cluster, and all connected menisci have the same curvature (Eq. 17 in Table III).

The equations, except those for liquid mass balance at pore bodies, contain both the unknowns and their time derivatives. Thus they are ordinary differential equations. The liquid balances at pore bodies are called algebraic equations because they lack time derivatives. The differential–algebraic-equation system was integrated in time by DASRT[1] *(30)*, in which PGMRES[2] *(31)* was used to solve the sparse matrix problem as it evolved from Haines jump to Haines jump. The integration is stopped at each Haines jump. After the equations of liquid redistribution by the jump are solved, the differential–algebraic-equation system is appropriately modified, and the integration is restarted until the next Haines jump. The whole computation for each case takes up to 15 hours on a Cray-2 computer.

[1] A differential-algebraic system solver with root finding.
[2] A preconditioned gerealtized minimal residual solver.

Results and discussion

The competitions between capillary-pressure-gradient driving force and viscous resistance and between binder convection and diffusion have been investigated. Drying rate, W, and binder-diffusion coefficient, D_b, used in the computations range from uncommonly low to unusually high values, as seen in **Table IV**. The values chosen may not be entirely realistic, but they bracket those encountered in practice. Consequently, predictions based on these values should be instructive.

Drying rate

Figure 7 shows drying rates in units of initial drying rate vs. fraction of liquid evaporated. The Sherwood number, Sh,

$$\mathrm{Sh} \equiv WL/\rho_v D_v$$

measures the ratio of internal to external resistance to vapor transfer. Here the coating is ten layers thick, or about 60 μm. The Sherwood number varies from 10^{-4} to 1 as drying rate varies between 0.1–1000 kg/m²·h in the thin coating. A small Sherwood number indicates that the relatively high external resistance to mass transfer dominates over the vapor transfer from inside the coating to the surface. The lowest initial drying rate considered corresponds to external mass-transfer resistance that remains much higher than the growing diffusional resistance in the pore space throughout the drying process. Hence in this case, the drying rate is constant, as in Croll's experiments with thin granular coatings in very gentle breezes *(32)*.

As the air flow velocity—and hence the mass-transfer coefficient and initial drying rate—is raised, the internal diffusional resistance at each stage of drying grows more important compared with the external resistance, and so the drying rate falls. The computed results show that the drying rate falls to about 80% at the end of drying from an initial drying rate of 100 kg/m²·h and to about 40% from an initial drying rate of 1000 kg/m²·h. Greater drops of drying rate at late drying stage have been observed *(33)*, which indicates that mechanisms are active that are not yet considered in the network model. Of these mechanisms, the occlusion of pore passages by deposited binder and the shrinkage of pore passages by capillarity-induced drying stress and latex coalescence are probably the most important *(10)*. The consequent "skinning" *(34)* can greatly impede diffusion of vapor through the pore space and thus reduce drying rate.

Liquid distribution

Figures 8 and 9 are snapshots of liquid distribution in the same coating during drying at low and high drying rates, respectively. The saturation (50%) is the liquid volume fraction in the pore space of the network. At every stage, the liquid distributes irregularly over the 1000 pore bodies because of the randomness of the pore-throat size distribution and the consequent randomness of Haines jumps. Pores are emptied of liquid from both the evaporating side of the coating and the bottom side. Initially, all of the liquid is connected in a single cluster, but as evaporation and emptying proceed, the liquid breaks up into more and more smaller clusters bounded by smaller pores. In the late stages of drying, the small clusters progressively shrink and disappear. The last clusters are in the smallest pores deep within the coating, where their evaporation is impeded by the diffusional resistance to vapor movement.

At the lowest drying rate considered here, the capillary driving force of liquid movement is much larger than the viscous resistance, and as a result the largest pores accessible to vapor empty first, and thereafter, in each liquid cluster, they empty in the order of decreasing size accessible to vapor. At higher drying rates, the relative importance of viscous resistance is larger. The liquid that has evaporated from menisci at or

near the top surface cannot be replenished fast enough, and so those menisci tend to reach their nearby pore throats, jump, and empty the passage and pore body ahead of liquid at an earlier stage of drying. A consequence is that those menisci have less time to suck liquid out of the lower part of the coating, and so they leave more liquid-filled pores in the lower part.

Liquid distribution in a drying paper coating correlates with the capillary number, Ca, which represents effects of drying rate, suction by the action of capillarity, and viscosity:

$$Ca \equiv (\mu WL)/[\sigma\rho_l r_2(1 - ß)]$$

The maximum capillary pressure difference, $2\sigma[(1/r_{min}) - (1/r_{max})]$, gives the minimum capillary number, Ca_{min}. The minimum capillary pressure difference, $2\sigma\{(1/r_1) - [1/(r_1+\partial r)]\}$, arises between the pore throats of closest size and gives the maximum capillary number, Ca_{max}. If both Ca_{min} and Ca_{max} are small, as in the case of slow drying (Fig. 8), the pores bounding each liquid cluster at every stage empty of liquid in the order of decreasing size. If Ca_{max} is large and Ca_{min} is small, as in the case of fast drying (Fig. 9), the chances are greater that pores in top layers empty of liquid sooner. The results imply that when Ca_{min} and Ca_{max} are both large, liquid has little opportunity to flow. The result is that menisci recede only by evaporation and thus descend steadily along a fairly uniform front, i.e., drying is from the top down.

Binder migration

At rapid drying rates, pores near the top of the coating tend to empty sooner. Earlier results from a two-dimensional model *(29)* showed that evaporation within the top pores was more rapid, with binder concentrating and depositing sooner than at slower drying rates when the binder diffusivity was the same.

Figure 10 is a snapshot of binder deposition in the top two layers and the bottom two layers of a coating at the very fast drying rate of 1000 kg/m²·h. When the drying rate is high and the binder diffusivity is great (Case 4), more pores near the top of the coating empty of liquid before the binder reaches saturation and deposits. Consequently, when drying is rapid, and binder diffusivity is great, lateral distribution in the top layers tends to be spotty. However, in those liquid-filled pores adjacent to evaporating menisci that have not jumped for a while, the deposition is very heavy. On the other hand, binder has more time to concentrate and deposit in more pores near the bottom that are still liquid-filled until the late stage of drying.

Figure 11 shows the binder deposition in the top two layers and the bottom two layers of a dried coating when the drying rate was slow and the binder diffusivity was high (Case 3). Binder diffusivity is so adjusted that the Peclet number is 0.001, the same as in the foregoing case, i.e., both drying rate and binder diffusivity are 10^4 times smaller in Fig. 11 than in Fig. 10, but diffusion is relatively fast in both cases. At the slower drying rate, more pores in the top two layers remain liquid-filled when the binder reaches saturation and deposits, although the deposition is light in many pores because they soon emptied of liquid.

Thus the deposition of binder is governed by the interplay of drying rate and binder mobility. **Figure 12** shows the binder deposition at slow drying and slow diffusion (Case 1). Because binder diffuses away very slowly from evaporating menisci, it concentrates there and deposits, while the binder concentration elsewhere is still near the initial value. Thus at about 50% liquid saturation, almost all pores in the top two layers have at least some binder deposited (Fig. 12A). In contrast, highly mobile binder is only lightly deposited in some pores during slow drying (Fig. 11A) because it just reaches saturation throughout the liquid. This comparison of binder deposition at slow drying was continued until the end of drying (Fig. 11, fast diffusion; Fig. 12, slow diffusion). Results of fast drying (Fig. 10, slow

14. Binder deposition, layer-by-layer, as multiple of saturated binder concentration. The value for a layer is the average over all its pores. The initial concentration is 50% of its saturation value. The conditions for Cases 1–5 are defined in Table IV.

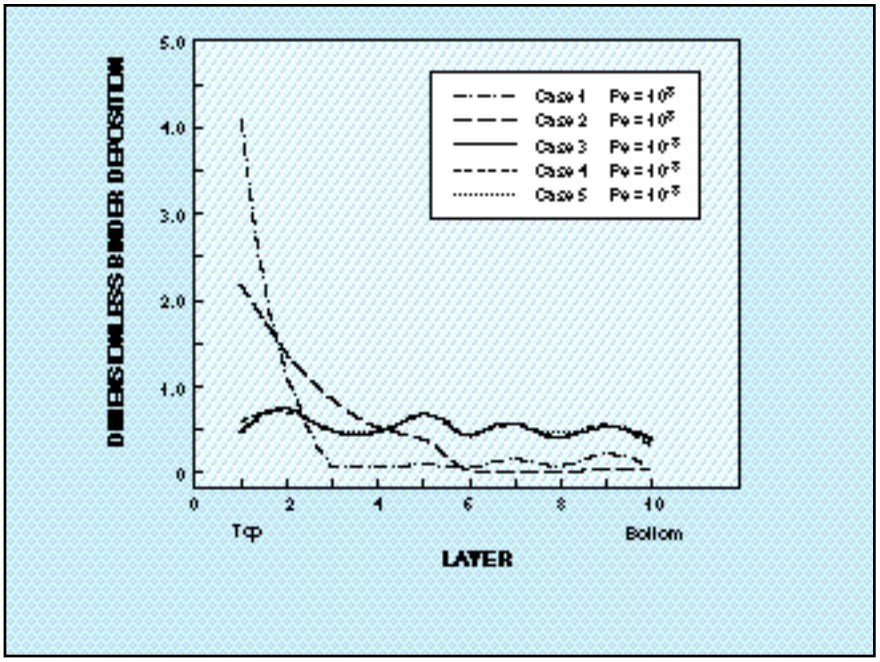

15. Illustration of the effects of initial drying rate and binder diffusivity on binder migration in paper coatings

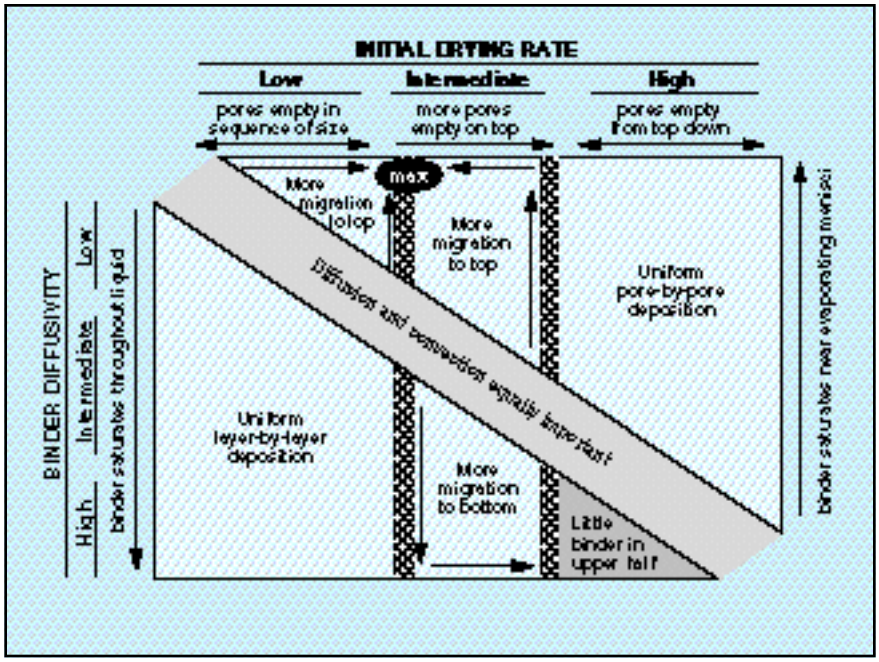

diffusion; **Fig. 13**, fast diffusion) show a similar effect of binder mobility. **Figure 14** summarizes binder deposition for the five cases described in Table IV.

From the foregoing results—and a more systematic study nearing completion *(35)*— the effects of drying rate and binder diffusivity on binder distribution are a little complicated, as shown qualitatively in **Fig. 15**. In the upper portion of the triangle at the right, drying is significantly faster than diffusion, so that raising the drying rate enhances binder migration to the coating surface. Binder migration reaches a maximum at some drying rate. Thereafter, migration actually becomes less severe until the rate becomes so high that coating dries from top down and binder deposits uniformly where liquid evaporates. The existence of the maximum explains why raising the drying rate does not necessarily promote binder migration, as is evident from Cases 1 and 2 (Fig. 14). In the lower portion of the triangle at the left, binder diffusivity is high and drying rate is comparatively low, so that binder can saturate and deposit only in the lower part of the coating. Reducing diffusivity enough always results in binder migration to the coating surface.

Binder distribution in a drying paper coating correlates with a Peclet number, Pe,

$$\mathrm{Pe}_b \equiv WL/\rho_1 D_b$$

which represents the competition between convection and binder diffusion. Figure 14 shows binder deposition profiles at low and high Peclet numbers. Binder deposition in a layer is averaged over all pores in that layer. At the low values, the average layer-by-layer binder deposition is about the same, from top to bottom. At the high Peclet number (high drying rate or low binder diffusivity), binder migrates to the coating surface. This result agrees with experimental observations *(7, 27)*. However, this correlation of binder deposition in paper coatings is incomplete without the effect of capillary number. The liquid distribution within the pore space correlates with the capillary number, as described in the preceding section. Actually, the effects of drying rate and binder diffusivity can be correlated with capillary number and Peclet number, as shown qualitatively in **Fig. 16**. The somewhat curved, broken lines suggest contours of roughly the same binder uniformity (or maldistribution). The diagonal corridor of uniform distribution is noteworthy.

Conclusion

The mechanism-based, three-dimensional network model of drying porous coatings shows how capillarity-driven liquid flow affects drying by distributing the liquid that remains at each stage. The effect plainly depends on the pore-size distribution of the coating, although that effect is not explored quantitatively here. It also depends strongly on initial drying rate (i.e., mass-transfer coefficient), liquid surface tension, and viscosity.

These parameters are all accounted for in a single correlating quantity, the capillary number of drying. (Pore size distribution is reflected in maximum and minimum capillary numbers, defined here as auxiliary quantities.) In the normal drying conditions of paper coating (Table I), this capillary number tends to be small, capillarity tends to dominate, and pores tend to empty in order of diminishing size of those accessible to air at each stage from Haines jump to Haines jump. It follows that in ordinary practice, there is little that can be done to manage the course of liquid distribution in a given paper coating as it dries.

The mechanism-based network model also shows how binder mobility influences its distribution, both in the remaining liquid cluster or clusters at each stage, and its deposition in the pore space. This influence depends on the effective diffusivity of the binder, which is quite low in the case of colloidal poly-

mer and rather greater in the case of soluble binder. The influence of the binder mobility also depends on the initial drying rate, which affects the distribution of binder-containing liquid with time and thus its local residence time.

These latter parameters—binder diffusivity and initial drying rate—are accounted for in a second correlating quantity, the Peclet number of binder distribution in drying coatings. It appears that in normal conditions of paper drying, this Peclet number ranges around unity and can be varied substantially by changing drying rate and binder mobility, the latter through choice and blend of binder and thickeners and through adjustment of temperature. Such control of binder migration as is exercised in ordinary drying practice is probably achieved through the Peclet-number effects examined here. On the other hand, although the mechanisms in the proposed network model are surely major ones, there are others not yet incorporated that may be important, particularly in the later stages of drying. These include effects of pendular liquid in nooks and crannies, thin films on surfaces, absorbed or bound water, nonuniformity of and dewatering by the substrate, gelation and skinning of soluble binders, flocculation and coalescence of particulate binders, and coating deformation and shrinkage.

16. Qualitative correlation of binder distribution with capillary number and Peclet number. Broken lines: roughly constant uniformity of binder distribution.

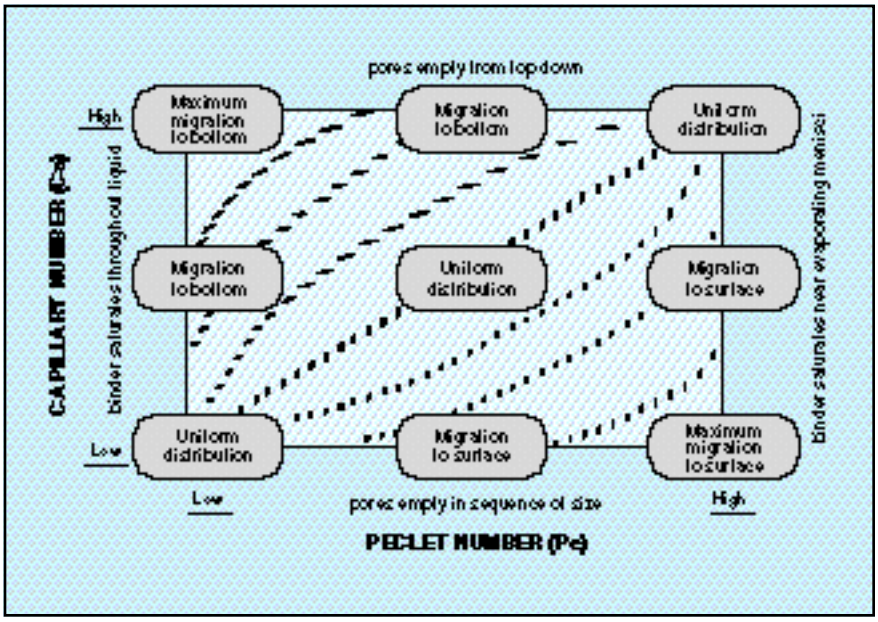

Literature cited

1. Watanabe, J. and Lepoutre, P., *J. Appl. Polymer Sci.* 27: 4207(1982).
2. Stanislawska, A. and Lepoutre, P., *Abstr. Papers ACS* 207(PMSE): 159(1994).
3. Alince, B. and Lepoutre, P., *J. Colloid Interface Sci.* 76(2): 439(1980).
4. Eklund, R. W., Erickson, L. D., and LeBlanc, H. A., *Tappi J.* 73(5): 153(1990).
5. Engström, G. and Rigdahl, M., "Effect of printability and print quality," in *Binder Migration in Paper and Paperboard Coatings* (M. J. Whalen-Shaw, Ed.), TAPPI PRESS, Atlanta, 1993, p. 61.
6. Dappen, J. W., *Tappi* 34(7): 324(1951).
7. Engström, G., Rigdahl, M., Kline, J., *et al.*, *Tappi J.* 74(5): 171(1991).
8. Hagen, K., "Effect of drying," in *Binder Migration in Paper and Paperboard Coatings* (M. J. Whalen-Shaw, Ed.), TAPPI PRESS, Atlanta, 1993, p. 39.
9. Nowicki, S. C., Davis, H. T., and Scriven, L. E., *TAPPI 1991 Coating Conference Proceedings*, TAPPI PRESS, Atlanta, 1991, p. 337.
10. Lepoutre, P., *Progr. Org. Coatings* 17(2): 89(1989).
11. Hemstock, G. A. and Bergmann, R. J., *Tappi* 51(11): 489(1968).
12. Trader, C. D., *Tappi* 54(10): 1709(1971).
13. Climpson, N. A. and Taylor, J. H., *Tappi* 59(7): 89(1976).
14. Lepoutre, P. and de Silveira, G., *J. Pulp Paper Sci.* 17(5): J184(1991).
15. Mohanty, K. K., Davis, H. T., and Scriven, L. E., *SPERE* 2.: 113(1987).
16. Purcell, W. R., *Petroleum Trans., AIME* 189: 369(1950).
17. McCabe, W. L., Smith, J. C., and Hariott, P., *Unit Operations of Chemical Engineering*, McGraw-Hill, New York, 1985, Chap. 25, p. 707.
18. van Brakel, J., "Mass transfer in convective drying," in *Advances in Drying* (A.S. Mujumdar, Ed.), Hemisphere, Washington, DC, 1983, p. 217.
19. Comings, E. W. and Sherwood, T. K., *I&EC* 26(10): 1096(1934).
20. Ceaglske, N. H. and Hougen, O. A., *Trans. Am. Inst. Chem. Eng.* 33: 283(1937).
21. Luikov, A. V., *Heat and Mass Transfer in Capillary–Porous Bodies*, Pergamon, London, 1966, Chap. 6, p. 233.
22. Whitaker, S., "Simultaneous heat, mass, and momentum transfer in porous media: A theory of drying," in *Advances in Heat Transfer* (T.J. Irvine and J.P. Hartnett, Eds.), Academic Press, New York, 1977, Vol. 13, p. 119.
23. Haines, W. B., *J. Agr. Sci.* 20: 97(1930).
24. Happel, J. and Brenner, H., *Low Reynolds Number Hydrodynamics*, 2nd edn., Martinus Nijhoff Publishers, Hingham, MA, 1973, Chap. 2, p. 23.
25. Cussler, E. L., *Diffusion: Mass Transfer in Fluid Systems*, Cambridge University, New York, 1984, Chap. 8, p. 194.
26. Hagen, K., *Tappi J.* 69(1): 93(1986).
27. Hagen, K., *Tappi J.* 72(5): 120(1989).
28. Engström, G., Ström, G., and Norrdahl, P., *Tappi J.* 70(12): 45(1987).
29. Pan, S. X., Davis, H. T., and Scriven, L. E., *Extended Abstr. AIChE*, American Institute of Chemical Engineers, New York, 1994, p. 102.
30. Petzold, L. R., *SIAM J. Sci. & Stat. Computing* 3: 367(1982).
31. Saad, Y. and Schultz, M. H., *SIAM J. Sci. & Stat. Computing* 7: 856(1986).
32. Croll, S. G., *J. Coatings Technol.* 58(734): 41(1986).
33. Graab, H., *Wochbl. Papierfabr.* 111(17): 645(1983).
34. Cairncross, R. A., "Solidification phenomena during drying of sol-to-gel coatings," Ph.D. thesis, University of Minnesota, Minneapolis, 1994.
35. Pan, S. X., "Modeling binder migration in drying porous coatings," Ph.D. thesis, University of Minnesota, Minneapolis, 1995.

The research was supported by the Coating Process Fundamentals Program through the Center for Interfacial Engineering and the Minnesota Supercomputer Institute of the University of Minnesota.

Received for review Jan. 24, 1995.

Accepted March 1, 1995.

Presented at the TAPPI 1995 Coating Conference.

Nomenclature

Variables

Bo = Bond number, the ratio of gravitational to capillary forces

c = concentration of binder

Ca = capillary number, the ratio of viscous resistance to capillary driving force

D_b = diffusivity of binder

D_v = diffusivity of vapor

g_L = local force of gravity

g_{ij} = liquid flow conductance between pore bodies i and j

k_m = mass transfer coefficient

l_{ij} = length of passage between pore bodies i and j

L = coating thickness

m = mass

M_b = molecular weight of binder

M_v = molecular weight of vapor

p = vapor partial pressure

P = pressure

Pe_v = Peclet number of vapor, the ratio of evaporative convection to vapor diffusion

Pe_b = Peclet number of binder, the ratio of convection rate diffusion rate in liquid

q = volumetric flow rate

r = radius of pore throat

R = radius of meniscus

R = universal gas constant

Re = Reynolds number, the ratio of the inertia of flow to viscous resistance

Sh = Sherwood number, the ratio of internal to external resistance to vapor transfer

t = time

T = temperature

V = liquid volume

W = initial drying rate

ß = pore size ratio, r_1/r_2

μ = liquid viscosity

ρ = density

σ = surface tension of liquid

Subscripts

a = air

b = binder

c = convection

d = diffusion

dist. = to be distributed

g = gas

i = pore body or meniscus or passage i

j = pore body or meniscus or passage j

k = pore body k

l = liquid

max = maximum

min = minimum

sat = saturated

v = vapor